Differential growth triggers mechanical feedback that elevates Hippo signaling

Yuanwang Pan[a], Idse Heemskerk[b], Consuelo Ibar[a], Boris I. Shraiman[b,1], Kenneth D. Irvine[a,1]

Supplementary Information

Simplified model of cell mechanics in epithelial tissue

The mechanical energy of a single cell subject to external compression can be described by

(1) $$E_c = T_c l + \frac{a_c}{A_c} + pA_c$$

where the 1st term represents the contribution of cortical tension T_c acting in the cytoskeletal cortex along the perimeter l of cell c. Cortical tension is generated by myosin activity. The second term represents internal pressure, which acts to increase the cell area A_c, (parameterized by a_c). Cell area A_c is proportional to l^2, with the exact relationship depending upon cell shape:

$A_c=\alpha l^2$

The last term in the expression for the mechanical energy (1) represents compression due to the pressure of the surroundings, which acts to reduce cell area. Given the energy as a function of *l,* equilibrium cell size is determined by minimizing *E* with respect to *l*. Equilibrium cell size evidently depends on T_c and *p*.

For an isolated cell, *p=0*, and the intrinsic cell size *l** would be determined by the balance of forces deriving from the 1st two terms:

(2) $$\frac{d}{dl}E_c = T_c - \frac{2a_c}{\alpha l^3} = 0$$

which is solved by

(3) $$l_* = (\frac{2a_c}{\alpha T_c})^{1/3}$$

Extending this calculation we can define the changes δl of equilibrium cell size in response to δp a small external pressure perturbation:

(4) $$\frac{d}{dl}E_c = \frac{6a_c}{\alpha l_*^3}\frac{\delta l}{l_*} + 2\delta p l_* = 0$$

The fractional change of cell size quantified by the strain $\delta l/l^*$, due to (small) external pressure δp would thus be given by

(5) $$\frac{3a_c}{\alpha l_*^3}\frac{\delta l}{l_*} = -\delta p l_*$$

Or equivalently by

(6) $$\frac{\delta l}{l_*} = -B^{-1}\delta p$$

where we defined an elastic modulus associated with the cell

(7) $$B = \frac{6a_c}{\alpha l_*^4} = \frac{3T_c}{2l_*}$$

More generally one can compute the strain induced by perturbation in both external pressure and cortical tension:

(8) $$\frac{\delta l}{l_*} = -B^{-1}\delta p - \frac{\delta T}{3T_c}$$

Observations suggest that adaptive response of the cytoskeleton, via myosin recruitment opposes deformation due to external forces. In the context of the present model this would correspond to cortical tension going down with increasing pressure (or *vise versa*) $\delta T_c = -kl\delta p$

(9) $$\delta T = -kl_*\delta p$$

with $k<1$ a coefficient parameterizing strength of adaptive response.

With such an adaptive response cell deformation induced by external pressure is smaller than what it would have been without it:

(10) $$\frac{\delta l}{l_*} = -B^{-1}\delta p(1-\frac{k}{2})$$

Note that the form of adaptive mechanical response used above is consistent with the Active Tension Network mode [l], which proposed that myosin recruitment into cortical cytoskeleton (and hence tension) depends on the rate of strain via:

(11)

$$T_c^{-1}\frac{d}{dt}\delta T = \kappa l_*^{-1}\frac{d}{dt}\delta l$$

This relation can be integrated in time leading to

(12) $$\frac{\delta T}{T_c} = \kappa\frac{\delta l}{l_*}$$

Which upon substitution into our equation (8) gives

(13) $$\frac{\delta l}{l_*} = -\frac{B^{-1}}{1+\frac{\kappa}{3}}\delta p$$

This also has the effect of reducing deformation in response to increase of external pressure (and we can identify 1-k/2=1/(1+κ/3)). We note that while adaptive mechanisms underlying (9) and (11) may be quite different on the molecular scale – in the former adaptation responds to change in pressure, in the latter it follows the deformation (or more precisely, the rate of strain) the net effect is the same: reduction of deformation in response to the perturbation. Note also that strain rate adaptation also leads to

(14) $$\delta T = -\frac{\kappa T_c B^{-1}}{1+\frac{\kappa}{3}}\delta p = -\frac{2l_*\kappa}{3+\kappa}\delta p$$

i.e. cortical tension goes down in response to increased external pressure. Note that the *coefficient* of proportionality between δT and δp is not important for the present argument, which was intended to demonstrate that rather general considerations of homeostatic adaptive response to external stress, which are consistent with the known myosin recruitment behavior, lead us to expect a reduction in myosin level and cortical tension in response to increased pressure.

Compression of overgrowing clones.

Let us now consider a clone of area A growing at a rate γ.

(15) $$\frac{d}{dt}A = \gamma A$$

This should be compared to the area of a clone with the background genotype

(16) $$\frac{d}{dt}A_b = \gamma_b A_b$$

Growing at the (slower) background rate $\gamma_b<\gamma$. It is evident that the overgrowing clone will have to be compressed by approximately $(A\text{-}A_b)/A$ factor – somewhat less actually on account of stretching of the surrounding tissue – because of the confinement constraint imposed by the tissue surrounding the clone. The expected "overpressure" compressing the overgrowing clone will be $\delta p \sim B(A\text{-}A_b)/A$. Importantly $(A\text{-}A_b)/A \sim \exp[(\gamma-\gamma_b)t]$ is growing exponentially with time. Hence we expect the effects of overgrowth and its consequences, such as adaptive reduction in cortical myosin/tension to become stronger with time.

Deformation due to an overgrowing clone.

It is instructive to work out explicitly the elastic deformation field induced by an expansion of disc-shaped region. We shall do it using classical continuum elasticity theory (see Landau and Lifshitz, [7]), by minimizing the elastic energy

(17) $$U = \int d^2\vec{r}\left[\frac{\mu}{2}(\partial_a u_b + \partial_b u_a - \delta_{ab}\partial_c u_c)^2 + \frac{B}{2}(\partial_c u_c)^2 - \gamma(r)\partial_c u_c\right]$$

Where $\gamma(r) = \gamma_0$ for $r<a$ and 0 otherwise, induces the expansion of the material within a disk of radius a. B and μ are the bulk and shear elastic moduli respectively. The resulting elastic displacement vector u_a obeys

(18) $$2\mu\partial_a^2 u_b + B\partial_b\partial_a u_a = \partial_b\gamma(r)$$

Which can be solved in terms of a 'scalar potential"

(19) $$u_a = \partial_a\phi$$

Upon substitution into the equation and integration we obtain

(20) $$\partial_a^2\phi = (2\mu + B)^{-1}\gamma(r)$$

which analogous to the calculation of electrostatic potential due to a uniformly charged disk (in 2D) and is solved by

(21) $$\phi = \frac{\gamma_0 r^2}{4(2\mu + B)} \quad \text{for } r < a \quad \text{and}$$
$$\phi = \frac{\gamma_0 a^2(1 + ln(r/a))}{4(2\mu + B)} \quad \text{for } r > a$$

From which we obtain the displacement vector

(22)
$$\vec{u} = \frac{\gamma_0 \vec{r}}{2(2\mu + B)} \quad \text{for } r < a \quad \text{and}$$
$$\vec{u} = \frac{\gamma_0 a^2}{4(2\mu + B)} \frac{\vec{r}}{r^2} \quad \text{for } r > a$$

We observe that the disc ($r < a$) region has undergone uniform expansion and is under pressure

(23)
$$p = B\partial_a u_a - \gamma_0 = \frac{2\mu\gamma_0}{2\mu + B}$$

In contrast, deformation in the region outside ($r > a$) has zero divergence and is described by a purely deviatoric strain tensor

(24)
$$\partial_x u_x = -\partial_y u_y = \frac{\gamma_0 a^2}{4(2\mu + B)} \frac{y^2 - x^2}{r^4}$$
$$\partial_y u_x + \partial_x u_y = \frac{\gamma_0 a^2}{4(2\mu + B)} \frac{4xy}{r^4}$$

(This corresponds to $p=0$ and a purely deviatoric stress, proportional to the strain defined above).

In the context of overgrowing clones (represented by an expanded disc) this corresponds to the radial flattening (and azimuthal elongation) of "cells" outside which decreases as $1/r^2$ with distance from the clone. Interestingly, according to this simple calculation, no anisotropy in cell shape is expected within the clone.

Supplemental Materials and Methods

Live Imaging and Laser Cutting of Cell Junctions

Live imaging and laser ablation experiments were performed as previously described [2]. To make discs with ban overexpressing clones, act>y+>Gal4 UAS-mCD8:RFP flies were crossed with y w hs-Flp; Ubi-Ecad:GFP; Gs-Bantam flies. Heat shocks were performed for 37°C 7 min to induce clones, and 2.5 days later wing discs were dissected at 108h ± 4h AEL. For making wild-type clones in *Minute/+* background, y w hs-Flp; tub-Gal4 UAS-mCD8:RFP; *Rps17*^{4} tub-Gal80 FRT80B/TM6B flies were crossed to y w-Flp; Ubi-Ecad:GFP; FRT80B flies. Similarly, heat shock was done for 10min at 37°C; 2.5d days later wing discs were dissected at 120h ± 4h AEL. In both cases, wing discs were cultured in WM1 media in a 4-well chambered coverglass (Nunc Lab-Tek II) coated with poly-lysine. Discs were imaged every 0.2 s on a Perkin Elmer Ultraview spinning disc confocal microscope, and ablation of junctions was achieved using a Micropoint pulsed laser (Andor) tuned to 365 nm. Paired cutting of junctions, one in the clone and another in a non-clone region at a similar location, were performed and compared in the wing discs. The displacement of vertices for the 1st second after ablation was used to calculate the velocities.

Image Processing and Quantitative Image Analysis

To compensate for aberrations due to the curvature of wing disc, clone induced distortions, and signals from the peripodial epithelium, we used the Matlab toolbox ImSAnE [3] to detect and isolate a slice of the disc epithelium surrounding the adherens junctions, using E-cadherin or Armadillo as a reference. ImSAnE projects a curved surface onto a flat surface. Projections of 5-7 ImSAnE generated surfaces (0.8-1.2 μm in total) surrounding the center of E-

cad or Arm were then used to identify the signal at this cell layer and create images showing for Sqh:GFP, Zip:GFP, Jub:GFP, F-actin and Wts:GFP localization.

Quantitation of junctional Jub:GFP, E-cad, Arm, F-actin, and Wts:GFP was performed as previously described [2], using Volocity (Perkin Elmer) software. In brief, E-cadherin or Armadillo was used as a junctional reference to define the volumes to be quantified. To compare Jub:GFP, F-actin and Wts:GFP between clone and the non-clone regions, we selected 10-20 cell regions of interest in the clone and defined mean fluorescence intensities overlapping adherens junctions; and identically sized objects were assayed in a non-clone region at an equivalent location in another compartment of the same disc. Quantitation of Yki, ban-lacZ, and ex-lacZ was performed similarly, except we quantified and compared their nuclear intensities, using DNA staining to define nuclei.

Since both junctional and apical myosins are affected by differential growth, and myosin is not completely enclosed within E-cad or Arm staining, we used a different method to quantify Sqh:GFP or Zip:GFP. Confocal stacks were first processed using ImSAnE to detect the apical surface. The processed 2D images were then quantified using ImageJ. An area containing 10-20 cells was selected in the clone to quantify the mean fluorescence intensities; and an identically sized region was selected in a non-clone region at an equivalent location in another compartment of the same disc.

Variability in mean ratios is presented using 95% confidence intervals, determined using GraphPad Prism6 software. Statistical comparisons between these mean ratios was performed by One-way Anova with Tukey's correction, on the log of the ratios, using GraphPad Prism6 software.

Cell anisotropy analysis (Fig 1)

To analyze cell anisotropy in and outside of clones (Fig 1D), confocal stacks were first processed by ImSAnE [3] to make 2D surface images. The processed images were then segmented using Ilastik software [5], and the segmented pictures were used to perform anisotropy analysis with a custom Matlab script. For quantification (Fig 1G-I), a standard measure of orientational order is the magnitude of the nematic order parameter (see e.g. [6]. In two dimensions, it is given by

$$S = \langle 2\cos^2\phi - 1 \rangle \tag{25}$$

where ϕ is the angle between the local orientation and the mean orientation and <..> denotes an average. Here we modify this to measure cell orientation relative to the clone boundary as a function of the distance, *d*, to the boundary:

$$S_d \equiv \frac{\langle a_c^2(2\sin^2\phi_c - 1)\rangle_d}{\langle a_c^2\rangle_d}. \tag{26}$$

Cells are labeled by *c* and the average is over cells in a bin centered at distance *d* from the clone boundary, and a_c is the cell anisotropy defined as

$$a = \frac{l_{\mathrm{maj}} - l_{\mathrm{min}}}{l_{\mathrm{maj}} + l_{\mathrm{min}}}, \tag{27}$$

where l_{maj} and l_{min} are the lengths of the major and minor axis of the cell.

The angle ϕ_c is between the normal to the clone boundary and the major axis of the cell, which would be 90 degrees when the cells are elongated tangentially to the clone boundary. The normal to the clone boundary is extended across the disk by taking the gradient of the distance function (Matlab 2013a, function bwdist) $\mathbf{n} = \nabla d/|\nabla d|$ and the angle ϕ_c is defined relative to it.

The graph in Fig 1H shows average S_d versus *d* for 29 clones. (Note, we take the distance function *d* to be signed, with positive sign outside and negative inside.) The scatter plot in 1I

shows S_0 vs. S_{15} for a large number of clones, where S_0 and S_{15} are averages at the boundary and 15 microns outside, both over 2 micron-wide bins.

Simulation of the extended vertex model.

We are simulating a vertex model with the energy

$$E = \sum_c \left[T_c l_c + \frac{a_c}{A_c} \right], \tag{28}$$

where c labels the cells, T_c is the perimeter tension, l_c the perimeter length, a_c a parameter controlling the preferred cell size, and A_c the cell area. In contrast to the conventional vertex model we shall treat T_c and a_c as dynamical variables with dynamics of T_c capturing the effect of myosin adaptation to local mechanical stress and dynamics of a_c capturing the effect of cell growth.

The simulation runs the following in a loop:

1. Relax to mechanical equilibrium
2. Update tension and preferred cell size parameters, T_c and a_c
3. Divide randomly chosen cells.

1. Relax to mechanical equilibrium

The energy is minimized with the GNU Scientific Library Multidimensional Minimizer, using Polak-Ribiere conjugate gradient algorithm. The pressure in each cell is then obtained from the work done by the cell under a dilation relative to the cell centroid:

$$p_c dA_c = -\sum_{i \in c} \frac{\partial E_c}{\partial \vec{r}_i} \cdot \delta \vec{r}_i, \qquad \delta \vec{r}_i = \lambda(\vec{r}_i - \vec{\bar{r}}_c)$$

$$\implies \qquad p_c = -\frac{1}{A_c} \sum_{i \in c} \frac{\partial E_c}{\partial \vec{r}_i} \cdot (\vec{r}_i - \vec{\bar{r}}_c) \tag{29}$$

2. Parameter update

The parameters of each cell are updated according to the rules:

- $a_c(t+1) = a_c(t) + \gamma_c dt$
  with γ the growth rate
- $T_c(t+1) = T_c(t) - k(p_c(t+1) - p_c(t))$

  with *k* the strength of tension adaptation

3. Division

The probability to divide per unit time depends on the cell area *p(A)*.

The total probability in some time step *dt* is then $P = 1 - (1-p)^{dt}$.

For each cell, at each timestep, a coin is flipped with probability *P*, and if heads, the cell is divided. One choice for the function *p(A)* that seems to work well is

$$p(A) = \Theta(N-4)\Theta(A - A_0)\frac{A^n}{A_0^n + A^n} \tag{30}$$

Where *Θ(x)* is one for *x>0* and zero for *x<=0.* Therefore there is no division below some minimal area or when the number of neighbors is less than five and the probability saturates to one at large areas.

When a cell is divided the direction of division is randomly picked and an edge is inserted orthogonal to it. The relation between mother (m) and daughter (d) parameters is

- $T_d=T_m$, tension is kept the same from mother to daughter
- $a_d=a_m/2^{3/2}$, to keep the total equilibrium area fixed. This rule is based on the fact that the equilibrium area of a cell is

$$A = \alpha l^2 = \alpha^{1/3} \left(\frac{2a}{T} \right)^{2/3} \quad (31)$$

where c is a factor encoding the perimeter squared to area ratio for a regular polygon of a given number of sides, e.g. $3^{1/2}/24$ for a hexagon. Holding T fixed, preserving the equilibrium area requires

$$A_m = A_{d1} + A_{d2}$$
$$\sqrt{\alpha_m} a_m = \sqrt{2\alpha_{d1}} a_d + \sqrt{2\alpha_{d2}} a_d,$$

and approximating that $\alpha_m = \alpha_{d1} = \alpha_{d2}$ we have the above rule.

Parameters used in the simulation

The parameters that were used for the simulation shown in Figure 2 are

- $\gamma=1$ inside the clone, $\gamma=0.1$ outside the clone
- $k=0.05$
- $dt=0.05$
- $A_0=1.3$, $n = 6$

With the initial coniditons

- $T_c=1/2$
- $a_c=1$
- hexagonal initial lattice, which with these parameters has $A = 4^{2/3}\sqrt{3}/24 \approx 1$

Matlab scripts for analysis and simulations have been deposited at Github (https://github.com/idse/mechanicalFeedback)

Supplemental Figures

Supplemental Fig. S1 Clones lacking evidence of tissue distortion

A) Wing disc with clones of cells labeled by the Tie-Dye technique [4] to illustrate faster growth induced by ban-expression. Neutral clones are labeled blue or green, ban-expressing clones are labeled red (and yellow due to overlap of red and green). B) Cell anisotropy analysis of wild-type clones in *Rps17*^{4}/+ background. Green lines indicate long axis of cell. In contrast to ban-expressing clones (Fig. 1D), no bias in cell anisotropy is observed along clone borders. C) Vertical section through a wing disc with wild-type clones in *Rps17*^{4}/+ background (marked by absence of ß-gal marker, blue). D) Vertical section through a wing disc with clones co-expressing ban and RNAi-E2f1, marked by BFP (blue). The invaginations associated with ban-expressing clones (Fig. 1E) are not observed.

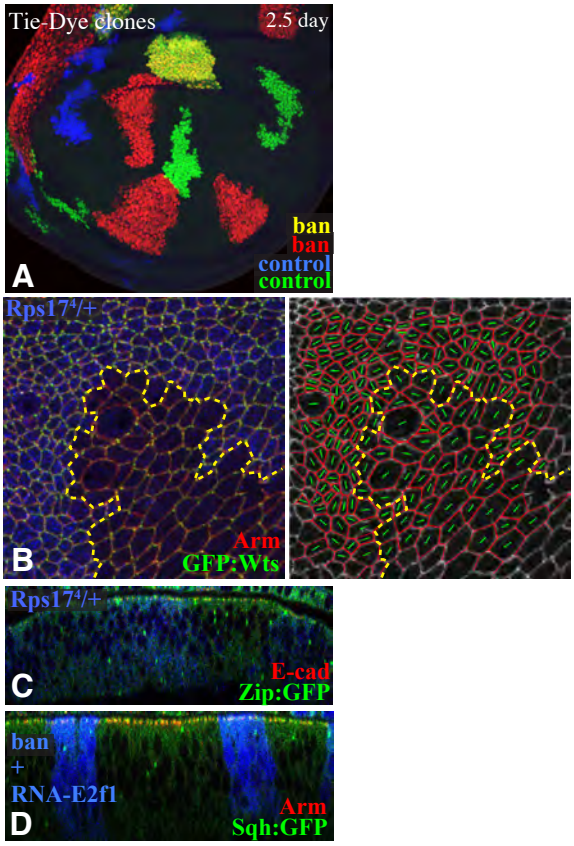
Tie-Dye clones
2.5 day
ban
ban
control
control
A
Rps17[4]/+
Arm
GFP:Wts
B
Rps17[4]/+
E-cad
Zip:GFP
C
ban
+
RNA-E2f1
Arm
Sqh:GFP
D

Supplemental Fig. S2 Additional analysis of myosin and F-actin

A) Wing disc with control clones grown for 2.5 days, labeled by expression of 2xBFP, with cell junctions labeled by Arm (red) and Myosin labeled by Sqh:GFP (green/white). B) Tabulation of relative levels of Myosin or F-actin, based on paired measurements inside of clones of cells of the indicated genotypes, compared to equivalent non-clone regions of the same discs, with variation indicated by the 95% confidence interval (CI); N indicates number of clones measured. C) Wing disc with clones expressing RNAi-E2f1 grown for 2.5 days, labeled by co-expression of 2xBFP, with cell junctions labeled by Arm (red) and Myosin labeled by Sqh:GFP (green/white). D) Wing disc with clones expressing RNAi-Myc grown for 2.5 days, labeled by co-expression of 2xBFP, with cell junctions labeled by Arm (red) and Myosin labeled by Sqh:GFP (green/white). E) Wing disc with clones of ban-expressing cells grown for 2.5 days, labeled by co-expression of 2xBFP, with cell junctions labeled by E-cad (red) and F-actin labeled by phalloidin (green). F) *Minute* heterozygous (*Rps17*^{4}) wing disc with clones of wild-type cells grown for 2.5 days, labeled by absence of ß-gal marker (blue), with cell junctions labeled by E-cad (red) and F-actin labeled by phalloidin (green).

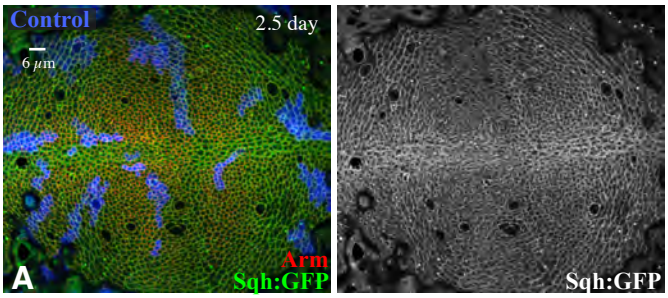

Relative Myosin level

Clone genotype	non-Clone genotype	GFP:MyoII Ratio	95% CI	N
wild-type	*wild-type*	0.993	0.030	13
UAS-ban	*wild-type*	0.801	0.036	14
wild-type	*Minute/+ (Rps17)*	0.828	0.033	14
UAS-Ras^{V12}	*wild-type*	0.817	0.071	13
UAS-ban RNAi-Myc	*wild-type*	0.967	0.020	15
UAS-ban RNAi-E2f1	*wild-type*	0.959	0.029	15
RNAi-Myc	*wild-type*	1.032	0.025	15
RNAi-E2f1	*wild-type*	1.016	0.023	15

Relative F-actin level

Clone genotype	non-Clone genotype	F-actin Ratio	95% CI	N
UAS-ban	*wild-type*	0.928	0.054	15
wild-type	*Minute/+ (Rps17)*	0.812	0.053	16

B

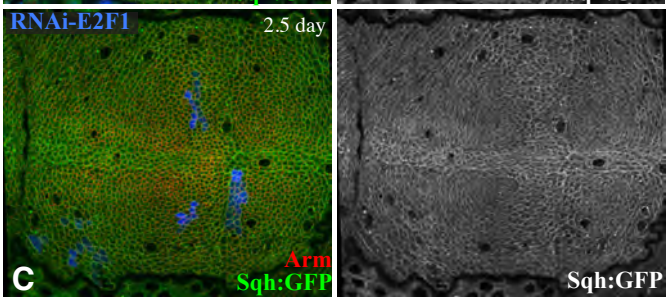

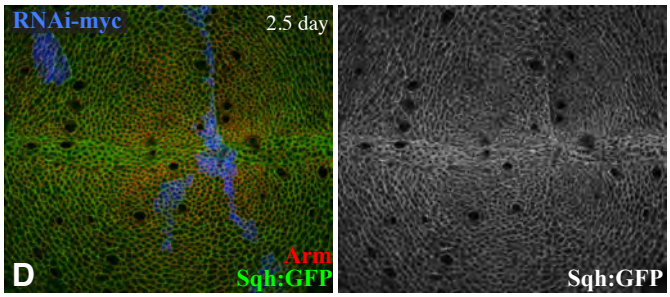

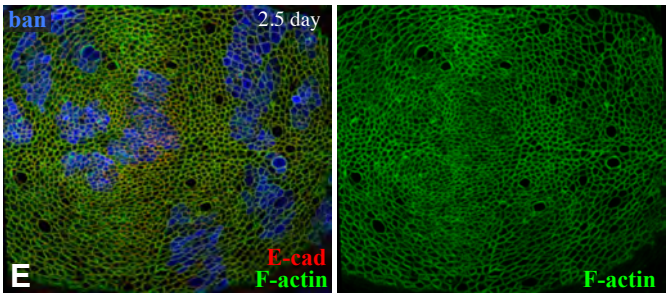

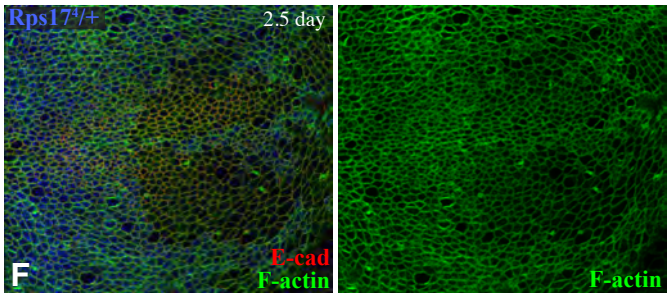

Supplemental Fig. S3 Additional analysis of Jub and Wts

A) Wing disc with control clones grown for 2.5 days, labeled by expression of 2xBFP, with cell junctions labeled by Arm (red) and Jub labeled by Jub:GFP (green/white). B) Wing disc with clones of ban-expressing cells grown for 2.5 days, labeled by co-expression of 2xBFP, with cell junctions labeled by Arm (red) and Jub labeled by Jub:GFP (green/white); Jub levels at junctions are decreased within clones. C) *Minute* heterozygous (*Minute(2)z*) wing disc with clones of wild-type cells grown for 2 days, labeled by absence of ß-gal marker (blue), with cell junctions labeled by E-cad (red) and Jub labeled by Jub:GFP (green/white); Jub levels at junctions are decreased within clones. D) Wing disc with clones of $ban^{\Delta 1}$ mutant cells grown for 2.5 days, labeled by absence of ß-gal marker (blue), with cell junctions labeled by E-cad (red) and Jub labeled by Jub:GFP (green/white). Mutant clone is outlined by dashed yellow line; Jub levels are unaffected. E) Wing disc with clones of RNAi-Myc-expressing cells grown for 2.5 days, labeled by co-expression of 2xBFP, with cell junctions labeled by Arm (red) and Jub labeled by Jub:GFP (green/white). F) Wing disc with clones of RNAi-E2f1-expressing cells grown for 2.5 days, labeled by co-expression of 2xBFP, with cell junctions labeled by Arm (red) and Jub labeled by Jub:GFP (green/white). G) Wing disc with control clones grown for 2.5 days, labeled by expression of 2xBFP, with cell junctions labeled by E-cad (red) and Wts labeled by GFP:Wts (green/white). H) *Minute* heterozygous ($Rps17^4$) wing disc with clones of wild-type cells grown for 2.5 days, labeled by presence of BFP marker (blue) using MARCM, with cell junctions labeled by E-cad (red) and Wts labeled by Wts:GFP (green/white); Wts levels at junctions are decreased within clones. I) *Minute* heterozygous ($Rps17^4$) wing disc with clones of cells expressing Sqh.EE grown for 2.5 days, labeled by presence of BFP marker (blue) using MARCM, with cell junctions labeled by E-cad (red) and Wts labeled by Wts:GFP (green/white). J) Tabulation of relative levels of junctional Jub, Wts, Arm or E-cad, based on paired measurements inside of clones of cells of the indicated genotypes, compared to equivalent non-clone regions of the same discs, with variation indicated by the 95% confidence interval (CI); N indicates number of clones measured.

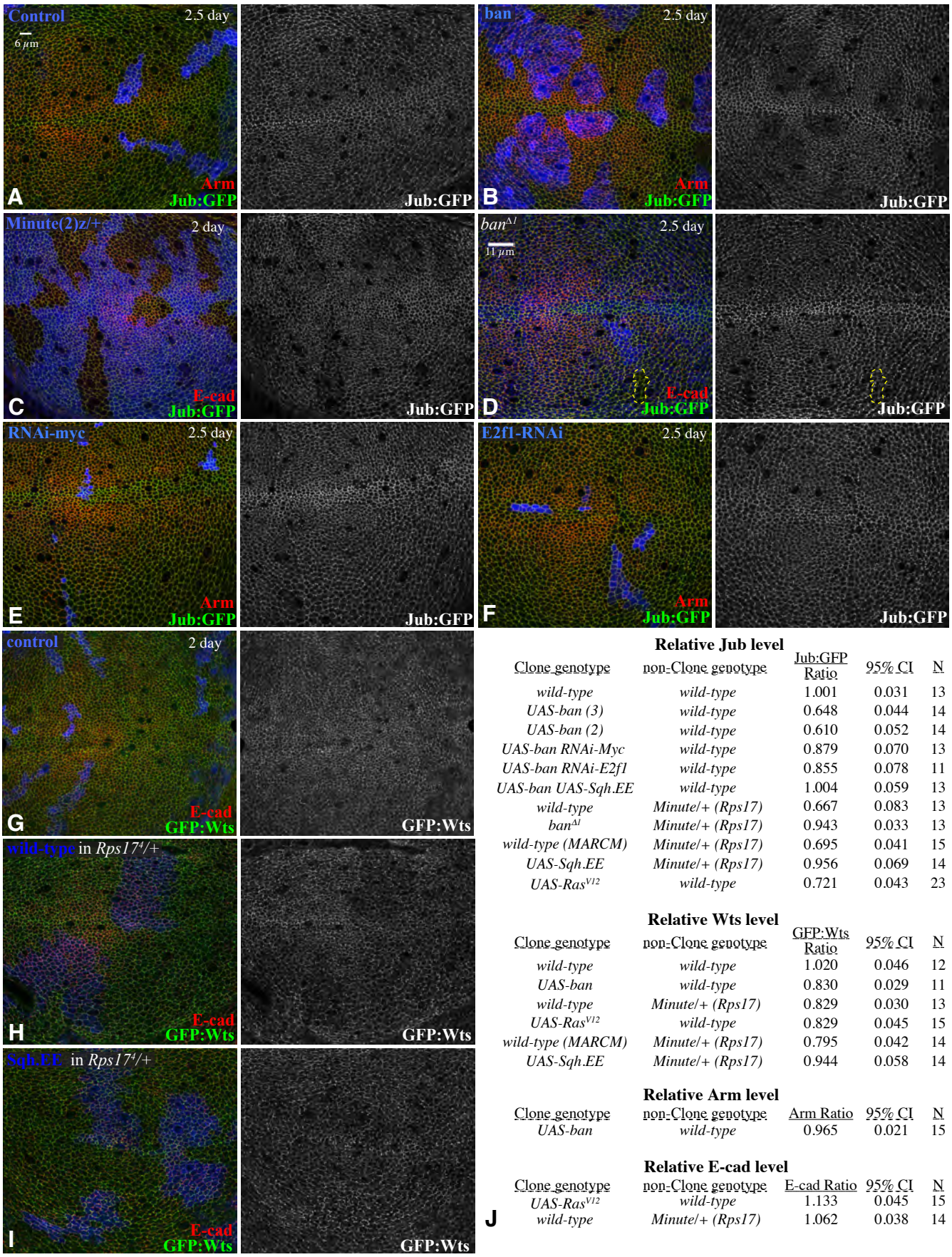

Relative Jub level

Clone genotype	non-Clone genotype	Jub:GFP Ratio	95% CI	N
wild-type	*wild-type*	1.001	0.031	13
UAS-ban (3)	*wild-type*	0.648	0.044	14
UAS-ban (2)	*wild-type*	0.610	0.052	14
UAS-ban RNAi-Myc	*wild-type*	0.879	0.070	13
UAS-ban RNAi-E2f1	*wild-type*	0.855	0.078	11
UAS-ban UAS-Sqh.EE	*wild-type*	1.004	0.059	13
wild-type	*Minute/+ (Rps17)*	0.667	0.083	13
$ban^{\Delta 1}$	*Minute/+ (Rps17)*	0.943	0.033	13
wild-type (MARCM)	*Minute/+ (Rps17)*	0.695	0.041	15
UAS-Sqh.EE	*Minute/+ (Rps17)*	0.956	0.069	14
$UAS\text{-}Ras^{V12}$	*wild-type*	0.721	0.043	23

Relative Wts level

Clone genotype	non-Clone genotype	GFP:Wts Ratio	95% CI	N
wild-type	*wild-type*	1.020	0.046	12
UAS-ban	*wild-type*	0.830	0.029	11
wild-type	*Minute/+ (Rps17)*	0.829	0.030	13
$UAS\text{-}Ras^{V12}$	*wild-type*	0.829	0.045	15
wild-type (MARCM)	*Minute/+ (Rps17)*	0.795	0.042	14
UAS-Sqh.EE	*Minute/+ (Rps17)*	0.944	0.058	14

Relative Arm level

Clone genotype	non-Clone genotype	Arm Ratio	95% CI	N
UAS-ban	*wild-type*	0.965	0.021	15

Relative E-cad level

Clone genotype	non-Clone genotype	E-cad Ratio	95% CI	N
$UAS\text{-}Ras^{V12}$	*wild-type*	1.133	0.045	15
wild-type	*Minute/+ (Rps17)*	1.062	0.038	14

J

Supplemental Fig. S4 Duration of ban clone growth correlates with loss of Jub

A,C,E Wing discs with clones of ban-expressing cells grown for 1 (A), 2 (B), or 3 (E) days, labeled by co-expression of 2xBFP, with cell junctions labeled by Arm (red) and Jub labeled by Jub:GFP (green/white). Decreased junctional Jub is visible after two or three days. B,D,F) Wing discs with clones of ban-expressing cells grown for 1 (B), 2 (D), or 3 (F) days, labeled by co-expression of 2xBFP, with ban activity revealed by GFP-ban sensor (green). For quantitation see Fig 4G.

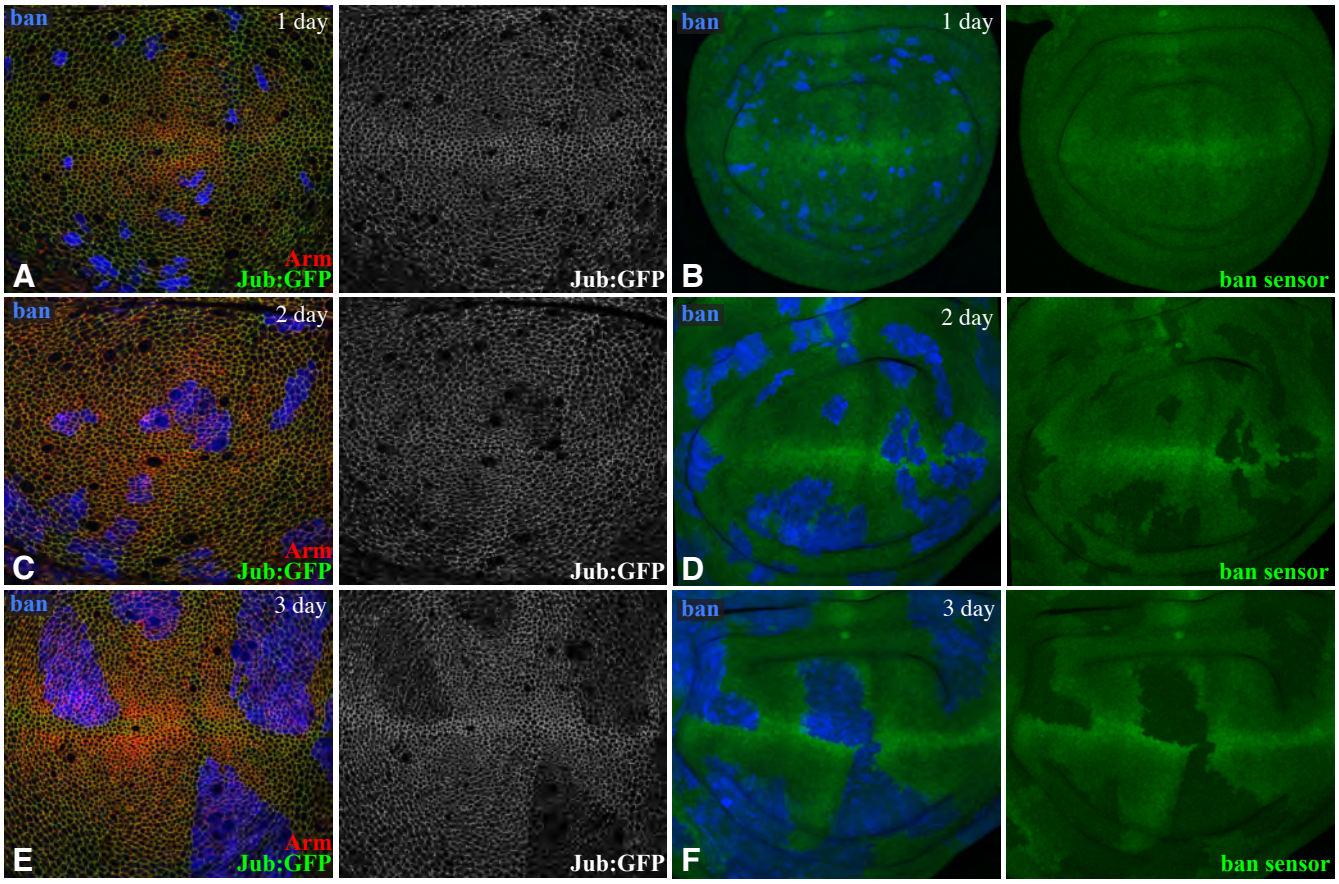
ban
1 day
Arm
Jub:GFP
A
Jub:GFP
ban
1 day
B
ban sensor
ban
2 day
Arm
Jub:GFP
C
Jub:GFP
ban
2 day
D
ban sensor
ban
3 day
Arm
Jub:GFP
E
Jub:GFP
ban
3 day
F
ban sensor

Supplemental Fig. S5 Additional analysis of Yki activity related to ban-expressing clones

Quantitation of the effects of these clones is provided in Supplemental Fig. S6E. A) Wing disc with clones of BFP-expressing cells (control) grown for 2.5 days, labeled by co-expression of 2xBFP (blue), stained for DNA (red) and ban-lacZ (green). B) Wing disc with clones of cells co-expressing ban and a UAS-RNAi construct targeting E2f1, grown for 2.5 days, labeled by co-expression of 2xBFP (blue), stained for DNA (red) and ban-lacZ (green). C) Wing disc with clones of cells expressing a UAS-RNAi construct targeting Myc, grown for 2.5 days, labeled by co-expression of 2xBFP (blue), stained for DNA (red) and ban-lacZ (green). D) Wing disc with clones of cells expressing a UAS-RNAi construct targeting E2f1, grown for 2.5 days, labeled by co-expression of 2xBFP (blue), stained for DNA (red) and ban-lacZ (green). E) Wing disc with clones of BFP-expressing cells (control) grown for 2.5 days, labeled by co-expression of 2xBFP (blue), stained for DNA (red) and Yki (green/white). F) Wing disc with clones of cells co-expressing ban and a UAS-RNAi construct targeting Myc, grown for 2.5 days, labeled by co-expression of 2xBFP (blue), stained for DNA (red) and Yki (green/white). G) Wing disc with clones of cells expressing a UAS-RNAi construct targeting E2f1, grown for 2.5 days, labeled by co-expression of 2xBFP (blue), stained for DNA (red) and Yki (green/white). H) Wing disc with clones of cells expressing a UAS-RNAi construct targeting Myc, grown for 2.5 days, labeled by co-expression of 2xBFP (blue), stained for DNA (red) and Yki (green/white). I) Wing disc with clones of BFP-expressing cells (control) grown for 2.5 days, labeled by co-expression of 2xBFP (blue), stained for DNA (red) and Diap1 (green). J) Wing disc with clones of cells co-expressing ban and a UAS-RNAi construct targeting E2f1, grown for 2.5 days, labeled by co-expression of 2xBFP (blue), stained for DNA (red) and Diap1 (green). K) Wing disc with clones of ban-expressing cells grown for 2.5 days, labeled by co-expression of 2xBFP (blue), stained for ex-lacZ (red).

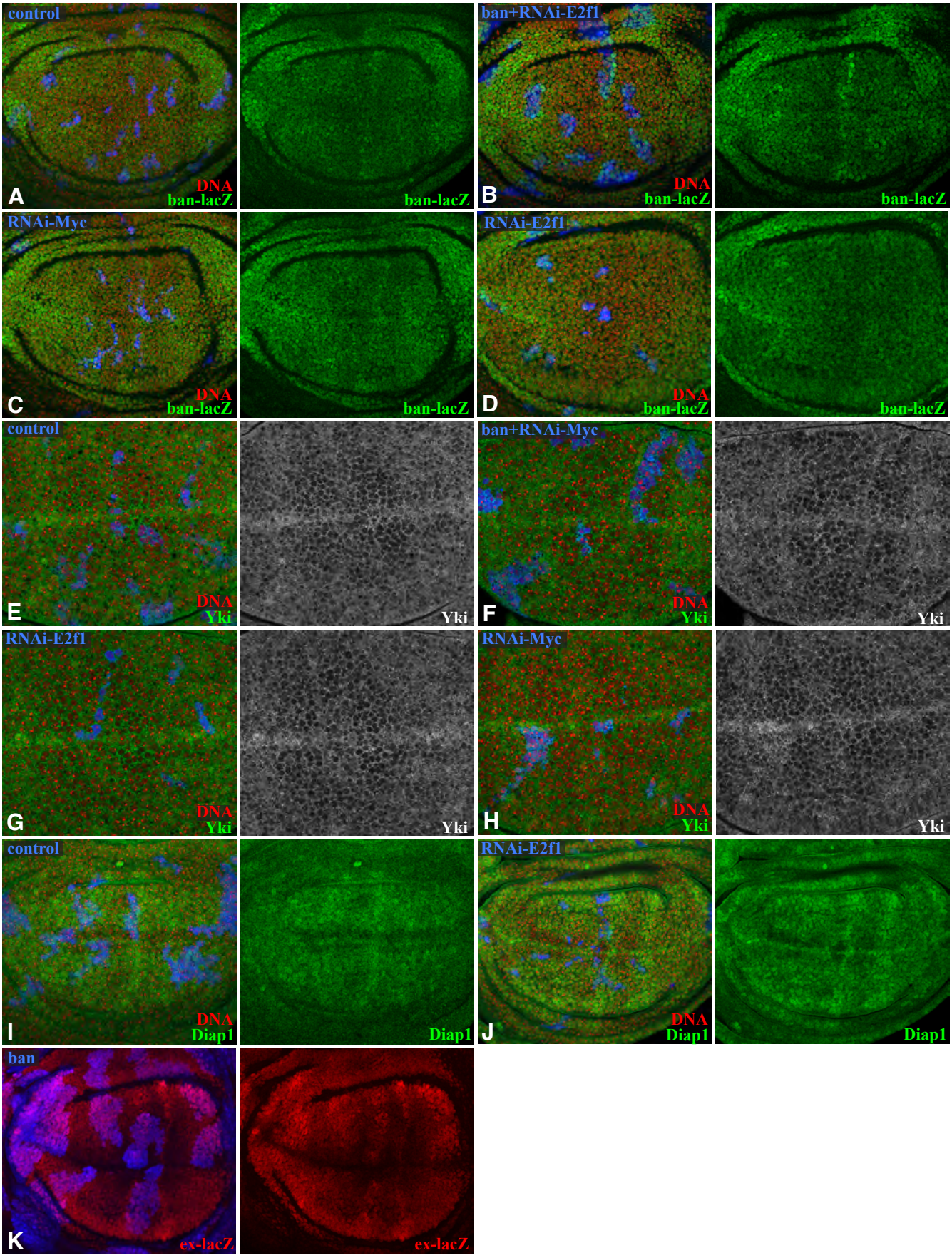
control
DNA
ban-lacZ
A
ban-lacZ
ban+RNAi-E2f1
DNA
ban-lacZ
B
ban-lacZ
RNAi-Myc
DNA
ban-lacZ
C
ban-lacZ
RNAi-E2f1
DNA
ban-lacZ
D
ban-lacZ
control
DNA
Yki
E
Yki
ban+RNAi-Myc
DNA
Yki
F
Yki
RNAi-E2f1
DNA
Yki
G
Yki
RNAi-Myc
DNA
Yki
H
Yki
control
DNA
Diap1
I
Diap1
RNAi-E2f1
DNA
Diap1
J
Diap1
ban
ex-lacZ
K
ex-lacZ

Supplemental Fig. S6 Additional analysis of Yki activity

A) *Minute* heterozygous (*Rps17*^{4}) wing disc with clones of wild-type cells grown for 2.5 days, labeled by presence of GFP marker (blue) using MARCM, and stained for DNA (green) and Yki (red/white). Thin panels above show vertical sections. Nuclear Yki levels are lower within the clones. B) *Minute* heterozygous (*Rps17*^{4}) wing disc with clones of cells expressing Sqh.EE grown for 2.5 days, labeled by presence of GFP marker (blue) using MARCM, and stained for DNA (green) and Yki (red/white). Thin panels above show vertical sections. C) Histogram showing relative levels of nuclear Yki in cells within clones of the indicated genotypes, as compared to cells outside of the clones at similar proximal-distal locations within the same wing disc. Values and numbers of clones analyzed are tabulated in E. Comparisons of the significance (by One-way Anova) of differences between some of these mean ratios is indicated by the gray lines, **** indicates P<0.0001. D) Wing disc with clones of *ban*$^{\Delta 1}$ mutant cells grown for 2.5 days, labeled by absence of GFP marker (blue), and stained for DNA (green) and ex-lacZ (red). Mutant clones are outlined by dashed yellow line. E) Tabulation of relative levels of nuclear Yki, ban-lacZ, Diap1 and ex-lacZ, based on paired measurements inside of clones of cells of the indicated genotypes, compared to equivalent non-clone regions of the same discs, with variation indicated by the 95% confidence interval (CI); N indicates number of clones measured.

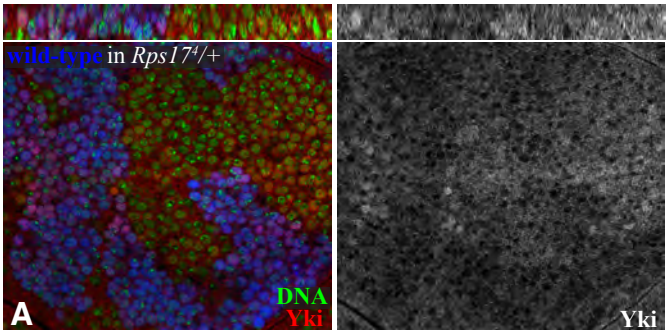

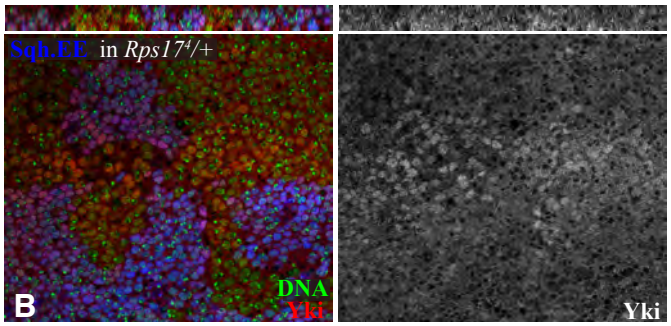

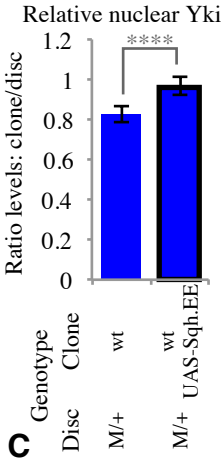

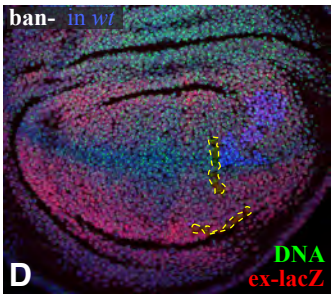

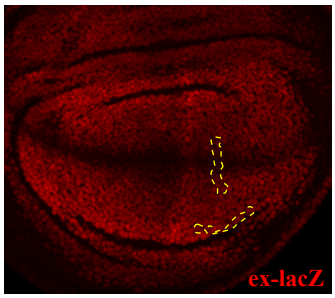

Relative nuclear Yki level

Clone genotype	non-Clone genotype	Yki Ratio	95% CI	N
wild-type	*wild-type*	1.014	0.039	14
UAS-ban	*wild-type*	0.632	0.021	15
UAS-ban RNAi-E2f1	*wild-type*	0.871	0.057	12
UAS-ban RNAi-Myc	*wild-type*	0.921	0.035	14
RNAi-E2f1	*wild-type*	0.987	0.034	14
RNAi-Myc	*wild-type*	1.131	0.063	12
wild-type	*Minute/+*	0.804	0.054	14
wild-type (MARCM)	*Minute/+*	0.821	0.040	14
UAS-Sqh.EE	*Minute/+*	0.995	0.042	14

Relative ban-lacZ level

Clone genotype	non-Clone genotype	ban-lacZ Ratio	95% CI	N
wild-type	*wild-type*	0.995	0.028	13
UAS-ban	*wild-type*	0.662	0.029	13
UAS-ban(2) RNAi-E2f1	*wild-type*	1.075	0.044	16
UAS-ban(3) RNAi-Myc	*wild-type*	1.014	0.047	16
RNAi-E2f1	*wild-type*	1.178	0.058	15
RNAi-Myc	*wild-type*	1.081	0.042	15
wild-type	*Minute/+ (M(2)25A)*	0.773	0.059	15
UAS-ban UAS-Sqh.EE	*wild-type*	0.861	0.030	14

Relative Diap1 level

Clone genotype	non-Clone genotype	Diap1 Ratio	95% CI	N
wild-type	*wild-type*	0.994	0.034	12
UAS-ban	*wild-type*	0.639	0.041	14
UAS-ban RNAi-E2f1	*wild-type*	0.9517	0.035	14
RNAi-E2f1	*wild-type*	0.990	0.025	12

Relative ex-lacZ level

Clone genotype	non-Clone genotype	ex-lacZ Ratio	95% CI	N
wild-type	*Minute/+ (Rps17)*	0.688	0.065	15
$ban^{\Delta 1}$	*Minute/+ (Rps17)*	0.917	0.041	15
$ban^{\Delta 1}$	*wild-type*	0.981	0.026	10

E

Supplemental Fig. S7. Summary and model

A) Summary cartoons illustrating the observed influences of some of the clones examined on growth, myosin, and Yki activity. Green indicates wild-type levels, red higher levels, and blue lower levels. B) Summary model illustrating that lower tension under conditions of higher cellular compression allows higher Wts activity, and thus lower Yki activity and reduced growth.

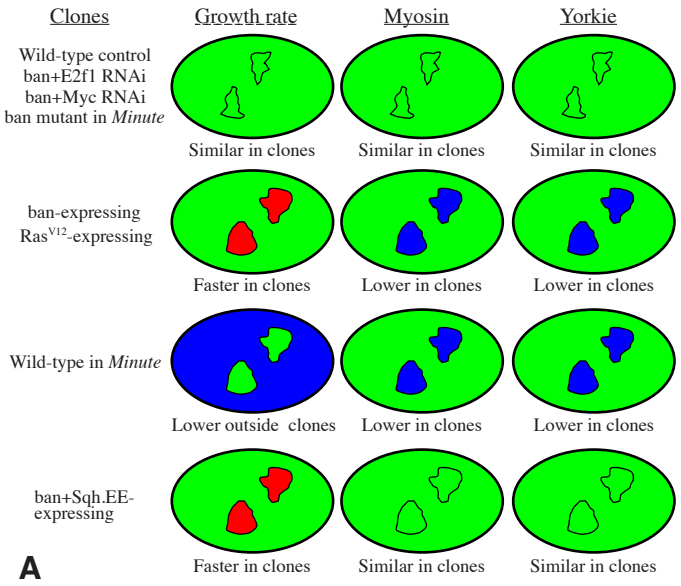
Clones
Growth rate
Myosin
Yorkie
Wild-type control
ban+E2f1 RNAi
ban+Myc RNAi
ban mutant in Minute
Similar in clones
Similar in clones
Similar in clones
ban-expressing
Ras^{V12}-expressing
Faster in clones
Lower in clones
Lower in clones
Wild-type in Minute
Lower outside clones
Lower in clones
Lower in clones
ban+Sqh.EE-expressing
Faster in clones
Similar in clones
Similar in clones
A

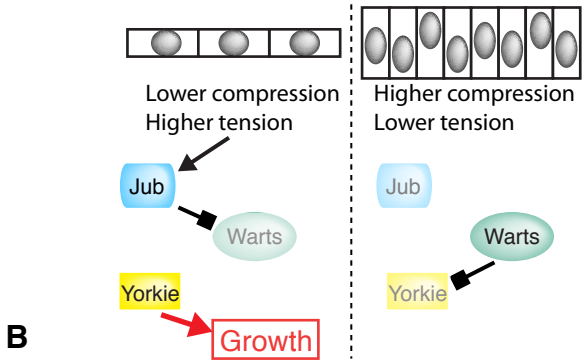
Lower compression
Higher tension
Higher compression
Lower tension
Jub
Warts
Yorkie
Growth
Jub
Warts
Yorkie
B

Supplemental Movies

Movie S1 Example of laser cut within ban-expressing clone

Junctions were cut within live discs with clones labeled by mCD8:RFP and junctions labeled by E-cad:GFP. See also Fig. 2E

Movie S2 Example of laser cut within wild-type cells

Junctions were cut within live discs with clones labeled by mCD8:RFP and junctions labeled by E-cad:GFP. See also Fig. 2E

Movie S3 Simulation of cellular pressure

Simulation showing altered cellular pressures that result from differences in growth rates, based on a modified vertex model. In this simulation, intrinsic cell size is larger for faster growing cells, pressure is increased as cells are constrained within an area smaller than their intrinsic size. Relative pressure is indicated by color scale (red=high, blue=low). See Fig. 2I, and Supplemental Materials and Methods, for details.

Movie S4 Simulation of cellular tension

Simulation showing altered cellular tensions that result from differences in growth rates, based on a modified vertex model. In this simulation, intrinsic cell size is larger for faster growing cells, pressure is increased as cells are constrained within an area smaller than their intrinsic size. Relative tension is indicated by color scale (red=high, blue=low). See Fig. 2I, and Supplemental Materials and Methods, for details.

Supplemental References

1. Noll N, Mani M, Heemskerk I, Streichan S, & Shraiman BI (2015) Active Tension Network model of epithelial mechanics. *arXiv*:arXiv:1508.00623 [q-bio.TO].

2. Rauskolb C, Sun S, Sun G, Pan Y, & Irvine KD (2014) Cytoskeletal tension inhibits Hippo signaling through an Ajuba-Warts complex. *Cell* 158:143-156.

3. Heemskerk I & Streichan SJ (2015) Tissue cartography: compressing bio-image data by dimensional reduction. *Nature Methods*.

4. Worley MI, Setiawan L, & Hariharan IK (2013) TIE-DYE: a combinatorial marking system to visualize and genetically manipulate clones during development in Drosophila melanogaster. *Development* 140(15):3275-3284.

5. Sommer, C., Straehle, C., Kothe, U., & Hamprecht, F. A. (2011). Ilastik: Interactive learning and segmentation toolkit (pp. 230–233). Presented at the 2011 8th IEEE International Symposium on Biomedical Imaging (ISBI 2011), IEEE. http://doi.org/10.1109/ISBI.2011.5872394

6. Principles of condensed matter physics, Chaikin, Paul M and Lubensky, Tom C, 2000, Cambridge university press Cambridge.

7. Theory of Elasticity, 3rd Edition, L.D. Landau, L. P. Pitaevskii, A. M. Kosevich and E.M. Lifshitz, 1986, Butterworth-Heinemann